CDDpress

www.nature.com/cddiscovery

ARTICLE OPEN

Genomic instability in individuals with sex determination defects and germ cell cancer

Maria Krivega[1✉], Jutta Zimmer[1], Anna Slezko[1], Petra Frank-Herrmann[2], Julia Rehnitz[2], Markus Hohenfellner[3], Markus Bettendorf[4], Marcin Luzarowski[5] and Thomas Strowitzki[2]

The ability to transmit genetic information through generations depends on the preservation of genome integrity. Genetic abnormalities affect cell differentiation, causing tissue specification defects and cancer. We addressed genomic instability in individuals with Differences of Sex Development (DSD), characterized by gonadal dysgenesis, infertility, high susceptibility for different types of cancer, especially Germ Cell Tumors (GCT), and in men with testicular GCTs. Whole proteome analysis of leukocytes, supported by specific gene expression assessment, and dysgenic gonads characterization, uncovered DNA damage phenotypes with altered innate immune response and autophagy. Further examination of DNA damage response revealed a reliance on deltaTP53, which was compromised by mutations in the transactivation domain in DSD-individuals with GCT. Accordingly, drug-induced rescue of DNA damage was achieved by autophagy inhibition but not by stabilization of TP53 in DSD-individuals' blood in vitro. This study elucidates possibilities for prophylactic treatments of DSD-individuals, as well as new diagnostic approaches of GCT.

Cell Death Discovery (2023)9:173 ; https://doi.org/10.1038/s41420-023-01470-6

INTRODUCTION

Mammalian gonads' specification is a unique process resulting in two very different organs systems from one bipotential progenitor. It is tightly regulated by a complex gene network providing specific conditions for cell lineages differentiation, followed by gonadal sex determination. Many of these genes are encoded on X and Y chromosomes and expressed in a dose-dependent manner [1].

It is now widely accepted that Y chromosome is susceptible to DNA deletions, which causes spermatogenic failure [2]. The instability of Y chromosome can be connected to the high frequency of repetitive DNA elements, which emphasizes the importance of DNA repair mechanisms to retain integrity of Y chromosome [3]. However, the inability to retrieve lost information because of the non-existent paired chromosome compromises a possibility of highly precise homologous recombination mechanism of DNA repair. As it was recently shown, artificially designed missegregation of Y-chromosome leads to its rapid loss from the cells [4]. It was accompanied by Y-chromosome isolation and shattering in the micronuclei, followed by an activation of the error-prone nonhomologous end joining (NHEJ) DNA repair mechanism. NHEJ further provokes genomic instability and increases levels of double-stranded brakes (DSB) in DNA, illustrated by highly sensitive epigenetic histone modifications [5]. The first steps of DNA repair are supported via phosphorylation of Histone protein H2AX on Ser139 (γH2A) to mark DSBs, and of TP53 to promote checkpoints for DNA repair [6]. This proper mechanism of DNA damage response (DDR) is critical for the genomic integrity of the entire cell and can be associated with the stability of the Y chromosome.

Abnormalities related to dysfunctional sex chromosomes are associated to Differences of Sex Development (DSD). In fact, two discoveries regarding DSD had shaped our current understanding of sex determination in humans. Identification of Turner (45,X0, females) and Klinefelter (47,XXY, males) syndromes defined the critical role of Y chromosome for a male differentiation [7, 8]. And much later, Y chromosome-specific SRY-gene translocation was shown to be sufficient to transform XX-individuals into males [9]. These days DSD is characterized by a large spectrum of complex conditions that among others include dysgenetic gonads (DG), gender specification, and inability to produce mature germ cells. Besides these severe infertility phenotypes, these individuals have a high risk to develop germ cell tumors (GCT) [10].

DGs are immature and contain remnants of primordial germ cells that are unable to differentiate and might lead to gonadoblastoma (GB), a primarily benign tumor with malignant capacity. DSD is described in individuals with Swyer syndrome (46,XY, females) that is often accompanied by GBs [11, 12]. Individuals carrying genetic mutations on Y-chromosomes have a 50% risk of developing Germ Cell Neoplasia in situ (GCNIS) and GB, and 50% can even develop into malignant tumors [13]. Alternative cases of 46,XY DSD-individuals possess 12-40% cancer risk [14]. In

[1]Research Group of Gonadal Differentiation and Embryonic Development, Department of Gynecological Endocrinology & Fertility Disorders, Women Hospital, University of Heidelberg, 69120 Heidelberg, Germany. [2]Department of Gynecological Endocrinology & Fertility Disorders, Women Hospital, University of Heidelberg, 69120 Heidelberg, Germany. [3]Department of Urology, University Hospital Heidelberg, 69120 Heidelberg, Germany. [4]Division of Pediatric Endocrinology, Children's Hospital, University of Heidelberg, 69120 Heidelberg, Germany. [5]Core Facility for Mass Spectrometry & Proteomics, ZMBH, University of Heidelberg, 69120 Heidelberg, Germany.
✉email: maria.krivega@med.uni-heidelberg.de

Received: 13 March 2023 Revised: 28 April 2023 Accepted: 12 May 2023
Published online: 23 May 2023

complete or partial androgen insensitivity syndrome (CAIS, PAIS, 46,XY, females) a malignant development is also increased with a 15% risk for adult women [15]. Women with Turner Syndrome carrying Y-chromosome material have 12-40% of GNIS/GBs and 3% dysgerminoma, and a risk for ovarian cancer [16]. Interestingly, men diagnosed with Klinefelter are known to suffer from mediastinal GCTs [17]. The strong resistance of these extragonadal tumors in comparison to gonadal GCTs is supported by P53 [18]. In addition to these observations, non-malignant GB was previously described as P53 positive [19]. Despite of significant efforts to identify the critical cancerogenic regions on Y-chromosome, the reasons behind the discrepancies among different groups of individuals with DSD and the driving force behind GBs transformation remain unclear.

A malignant differentiation of GB in dysgenic gonads was associated with the presence of Y-chromosome material, which might be the easiest target for genotoxic stress, as mentioned above. However, embryonal carcinoma can occur in women with karyotypes 45,XO and 46,XX due to the specific autosomal mutations, without the presence of Y-chromosome [20–22]. One should take into consideration, that non-DSD genetic syndromes e.g. Down syndrome (DS, Trisomy 21 chromosome), are often accompanied by delayed germ cell maturation resolving in testicular germ cell tumor (TGCT) [23]. These observations question the malignant activity of unstable Y-chromosome, and rather bring into focus the integrity of the entire genome.

The cellular defects associated with unbalanced karyotypes, including sex chromosome aneuploidy, may be caused by the disruption of cellular homeostasis due to the deregulation of genome-wide expression. Constitutive alterations of these genes cause a whole pleiad of cellular stress phenotypes including, but not limited to proliferation delay, defects in proteostasis, DNA damage and activation of innate immune response [24–27]. For example, Turner syndrome was associated with specific changes in a wide range of genes involved in cellular metabolism, immune response, genome methylation status, embryonic development and morphogenesis [28]. This leads to the susceptibility of DSD individuals to many other non-GCT types of cancer that go beyond reproductive tissues e.g. solid tumors of the skin and central neural system [29–31]. These cellular stress phenotypes were previously described in a context of genomic instability and aneuploidy in general [25, 32–35]. Therefore, in this work, we studied whether different groups of individuals with variations of their gonadal differentiation share common mechanisms which might cause an increased susceptibility to cancer.

RESULTS

Increased DNA damage levels in DSD-individuals

Compromised DNA integrity is a well-known sign of genomic instability, the leading cause of cancer. To evaluate general levels of DNA damage we analyzed leukocytes from the peripheral blood of 39 different DSD individuals with Swyer, CAIS, Turner and Klinefelter syndromes (Extended data table 1). For control, we used blood from fertile men and women (Extended data table 2). The ages of individuals from some DSD and control groups can vary since normal fertility was defined at regular childbirth age. Individuals with Swyer syndrome or CAIS who underwent gonadectomy for routine histological analysis formed an additional group with histologically proven GCT (DSD-GCT). Since the other two study groups do not usually undergo gonadectomy due to the established low risk of GCT occurrence, no gonadal tissue from these individuals was available for analysis.

DNA damage levels were estimated by assessing an increase of DSB via γH2AX. We identified more than two times upregulated γH2AX relative levels in leukocytes of individuals with Swyer syndrome (Fig. 1a–c), similar to those in DSD-GCT group. CAIS samples were not significantly different from a control (Fig. 1c, d). Interestingly, individuals with Turner and Klinefelter syndromes showed a pronounced increase by four times (Fig. 1c, e, f). As alternative confirmation of DNA damage we analyzed *H2AX* RNA expression [36]. We observed transcriptional upregulation, which was accompanied by over two folds increase in total H2AX protein levels exclusively in the DSD-GCT group (Fig. 1a, b, d–h).

To strengthen phenotypes described for DSD-GCT individuals, we included in our study an additional test group of 14 men diagnosed with TGCT (Extended data table 3). The leukocytes from peripheral blood uncovered a strong increase by six times in γH2AX and by two times in *H2AX* transcripts (Fig. 1i–k). In turn a slight increase in total H2AX protein levels was not statistically significant (Fig. 1i, l). Generally, we have not observed any significant correlation in DNA damage markers with increased age of control and DSD groups on protein levels (Extended data Fig. 1a, b). DNA damage levels were higher in individuals from DSD groups than from the control group at similar age. There was a correlation in control samples for *H2AX*, however, the fold changes were not higher than in DSD groups (Extended data Fig. 1c).

For further evaluation of a situation supporting compromised genome status, we performed mass spectrometry analysis for the entire proteome isolated from leukocytes of Swyer, CAIS and DSD-GCT groups. All the samples from DSD individuals were normalized to control and mainly showed upregulation of extracellular signaling in Swyer, and inflammatory response in group with GCT, however, pathways involved in RNA biogenesis, translation and oxidative mitochondrial processes were downregulated in DSD-GCT, or extracellular matrix was decreased in CAIS (Extended data Fig. 1d–f; Supplementary dataset 1). While there were generally more deregulated processes in GCT presence, observed phenotypes could potentially represent genotoxic stress and deregulated DNA damage repair mechanisms in all study groups (Extended data Fig. 1d–f). In turn some genes e.g. RPAB3, RPB1, RPB4, SNF5, RFC5, TRRAP, PARP9, H2A3 were downregulated in Swyer group with GCT and simultaneously upregulated in Swyer without GCT, likely representing requirement of specific DNA repair mechanisms for these individuals (Fig. 1m, Supplementary dataset 2).

Since we have not observed a tumor-specific difference for γH2AX, all of the DSD groups show tendency for DNA damage levels upregulation. However, differential expression of other genes, potentially implies the existence of specific mechanisms in GCT group, that could be related to DDR, which we will further investigate.

Dysgenic gonads contain cells with nuclear deterioration

Nuclear deformation and micronucleation illustrate severe problems with genome organization, chromosomal missegregation, aneuploidy and associated DNA damage [37]. As recently shown germ cell aplasia is also associated with nuclear indentation in gonads of infertile men [38]. Therefore, we analyzed the shape of the nuclear envelop in biopsied gonadal tissue of five Swyer and six CAIS individuals. For control, we studied testicular biopsies from fertile men with mature spermatogenesis (Fig. 2a). In contrast to control, individuals with Swyer syndrome had misshaped nuclei and multinucleation characterized by decreased circularity and roundness parameters, also with GCT (Fig. 2b–e). AMH-positive Sertoli cells of CAIS-individuals looked similar to the control, which reflected on the little decrease in nuclei circularity and roundness, likely illustrating the absence or little deterioration of genomic integrity (Fig. 2d–g). We also observed increased percentage of γH2AX positive cells, with upregulated number of puncta, in gonads of Swyer, DSD-GCT and TGCT-individuals, while CAIS syndrome was associated with little or no change (Fig. 2h–k).

The signs of compromised genome integrity in gonadal tissue supplement our data on peripheral blood and imply the presence of systemic problems causing DNA damage in individuals with DSD syndromes, except for CAIS group, whose phenotypes are caused by a specific Androgen Receptor gene mutation.

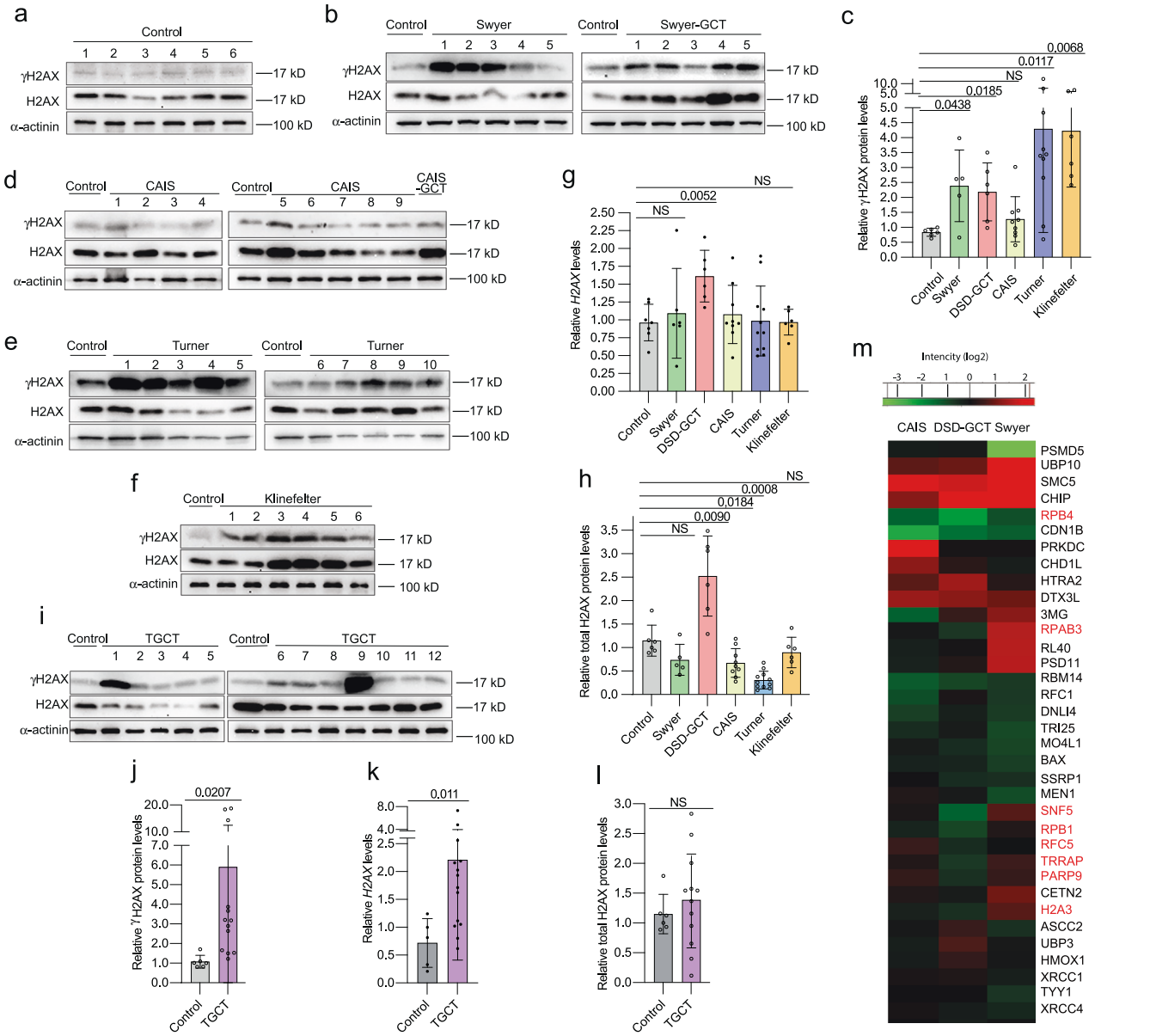

Fig. 1 DNA damage in leukocytes of DSD- and TGCT-individuals. Immunoblotting for γH2AX and total H2AX proteins from leukocytes of controls (**a**) and individuals with Swyer and Swyer-GCT (**b**). Quantification of relative γH2AX protein levels calculated for DSD-group (**c**). Immunoblotting for CAIS and CAIS-GCT (**d**), Turner (**e**), Klinefelter (**f**) syndromes. Relative gene expression of *H2AX* measured for DSD-group (**g**). Quantification of relative total H2AX protein levels normalized to α-actinin of DSD (**h**). Immunoblotting for TGCT-group (**i**) and its relative quantification (**j**). qRT-PCR for *H2AX* gene expression for TGCT-samples (**k**). Total H2AX protein levels normalized to α-actinin in TGCT-samples (**l**). **m** Heat map of GO selection on proteins involved in DNA damage repair from entire proteome of DSD-individuals, normalized to control. Red labeled proteins were upregulated in GCT samples compare to Swyer and/or CAIS groups. Unpaired t test was used for statistical analysis, p values are indicated.

Changes in innate immune response are associated with genotoxic stress in DSD- individuals

To estimate whether increased DNA damage has biological significance we examined changes in well-known DDR phenotypes. A number of cytoplasmic responses can be activated to alleviate deleterious consequences of genotoxic stress and support cell survival. Autophagy, regulating protein degradation, and type I Interferon signals were shown to reflect compromised integrity of genomic DNA in multiple cell lines and animal models. However, nobody has assessed this interplay in DSD samples.

In addition to inflammatory responses activation in DSD-GCT group (Extended Fig. 1e), we showed that wide range of proteins involved in immune response is deregulated in DSD individuals (Fig. 3a, Supplementary dataset 3). We observed particularly high levels of proteins e.g. KS6A2, APOL1, BRK1, BMX, RIPK3, APOA4 (Fig. 3a, labeled blue). MX1 was induced in DSD-GCT and CAIS, and OAS3 in CAIS groups, illustrating interferon β (IFNβ)-relevant immune response activation in these samples (Fig. 3a, labeled red). Interestingly RNA helicases DHX36 and DDX41 were inhibited in DSD-GCT (Fig. 3a, labeled green), potentially implying the redundant role of RNA regulation in innate immune response induction in patients with germ cell tumor. Additional proof of DDR in blood of DSD-GCT and TGCT individuals was a significant transcriptional upregulation of type I interferon *IFNβ* and interferon stimulating genes (ISG) *ISG15* and *ISG56* up to 15 folds (Fig. 3b–e). ISGs' induction was exclusively associated with GCTs, since CAIS-individuals with

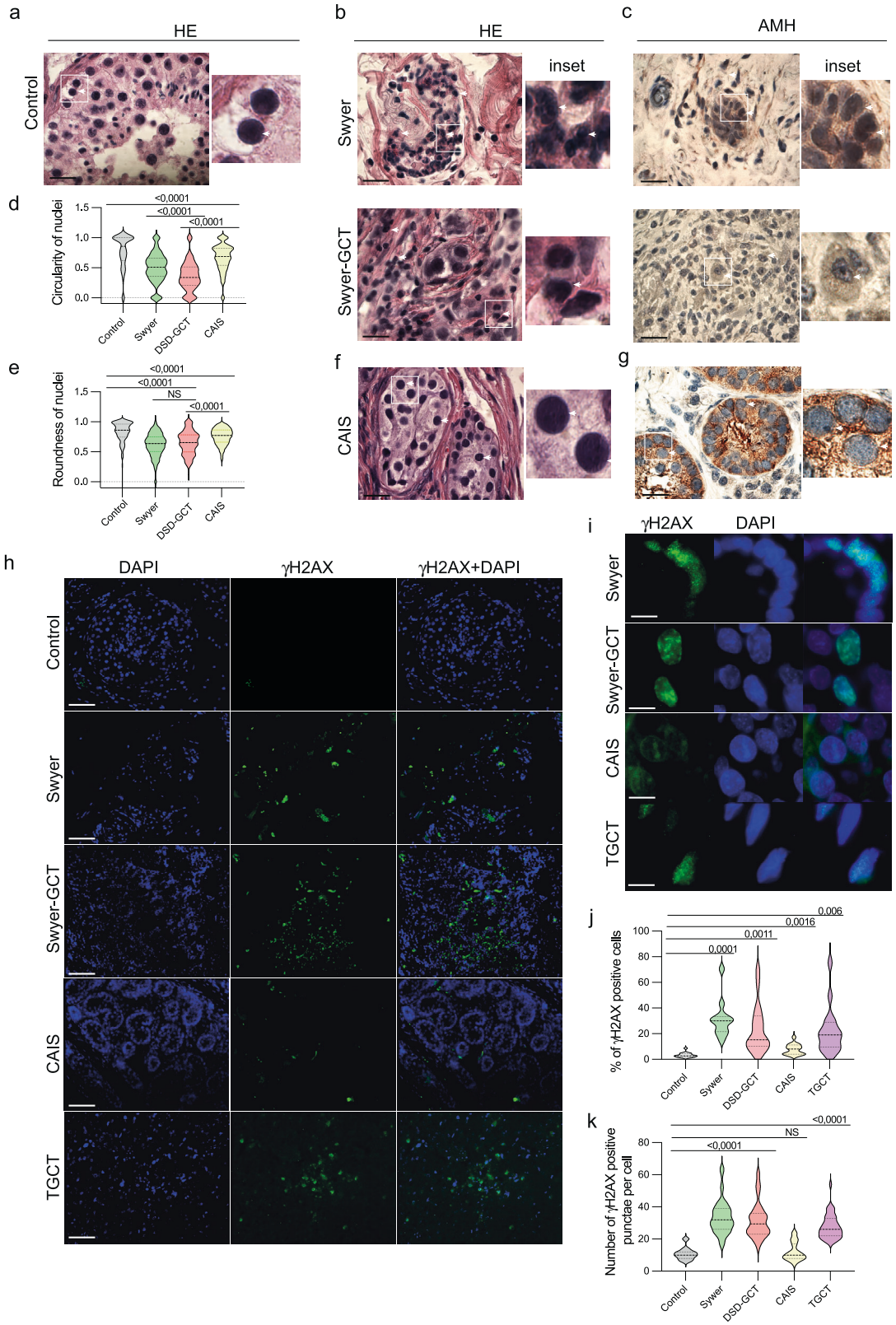

Fig. 2 Genotoxic stress phenotype in cells of gonadal tissue from DSD-individuals. Gonadal tissue was stained with Hematoxylin-eosin (HE) staining to define nuclei in control ($n = 210$) (**a**), Swyer ($n = 342$) and Swyer-GCT ($n = 186$) (**b**). Immunohistochemistry for AMH to define Sertoli cells in Swyer and Swyer-GCT(**c**). Plots for circularity (**d**) and roundness (**e**) of the nuclei in Sertoli cells of individuals with DSD. CAIS group ($n = 526$) staining for HE (**f**) and AMH (**g**); n-number of cells analyzed per each group. **h, i** Immunofluorescence for γH2AX, positive puncta are indicated by while arrows. **j** Quantification of percentages of γH2AX positive cells in control ($n = 16$), Swyer ($n = 11$), DSD-GCT ($n = 25$), CAIS ($n = 14$), TGCT ($n = 16$); n-number of images analyzed for each study group. **k** Quantification of number of γH2AX positive puncta in control ($n = 11$), Swyer ($n = 75$), DSD-GCT ($n = 46$), CAIS ($n = 33$), TGCT ($n = 40$); *n*-total number of cells analyzed in each group. Paired t test was used for statistical analysis, *p* values are indicated. Scale 10 μm (**a**–**c**, **f**, **g**), 2 μm (**h**), 0,4 μm (**i**). *n*-number of analyzed cells.

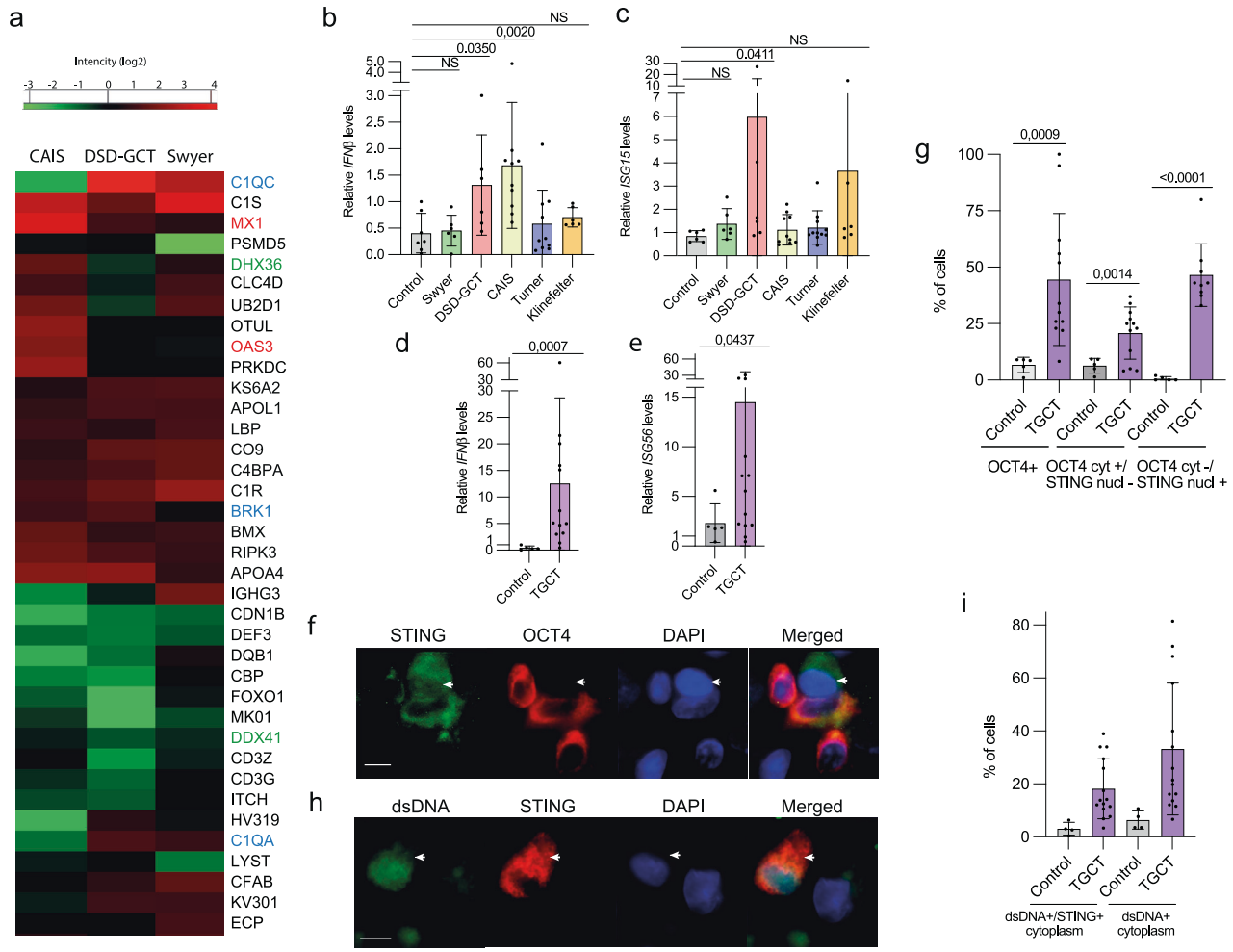

Fig. 3 Immune response in DSD and TGCT samples. Heat maps (**a**) represents a GO selection of immune response proteins from the entire proteome mass spectrometry data of leukocytes from individuals with DSD. Blue labeled the upregulated and green labeled the downregulated proteins in DSD-GCT, red labeled proteins are significantly upregulated in CAIS group. qRT-PCR data of innate immune specific gene expression in leukocytes of *IFNβ* (**b**), *ISG15* (**c**) for DSD group and *IFNβ* (**d**), *ISG56* (**e**) for TGCT group. Immune fluorescence analysis of TGCT gonadal tissue biopsy for STING and OCT4 proteins (**f**; n(TGCT) = 523; n(control)=871; arrow points to OCT4-negative non-GCT cell that has STING in the nucleus, in contrast to other OCT4-positive cells with STING exclusively concentrated in the cytoplasm) or dsDNA (**h**; n(TGCT) = 2140; n(control)=783; arrow points to colocalization of dsDNA and STING in the cytoplasm) and the quantification (**g**, **i**). Unpaired t test was used for statistical analysis, *p* values are indicated. Scale 0,4 μm (**f**, **h**). n-number of analyzed cells. Cyt cytoplasm; nucl nucleus.

inhibited androgen signaling only upregulated *IFNβ*. This observation additionally supports the potentially different character of immune response activation between DSD-GCT and CAIS groups.

In turn, *IL6* stimulated by alternative innate immune response pathway of nuclear factor kappa B (NFkB), was not altered in DSD-GCT (Extended data Fig. 2a). Importantly, we observed a positive correlation of *H2AX* and *IFNβ* transcripts in Swyer, Turner and TGCT-individuals (Extended data Fig. 2b, c). CAIS with low DNA damage levels didn't show similar correlation.

STING is critical for stimulating type I IFN response in a context of genomic instability. Therefore, we aimed to connect our finding in peripheral blood leukocytes with GCT cells. We analyzed gonadal tissue samples of men with TGCT and showed increased presence of OCT4 + GCT cells with active STING protein concentrating in the cytoplasm, where it functions to transmit the signal for innate immunity activation (Fig. 3f, g). While the cells with exclusively nuclear STING were negative for OCT4. Genomic dsDNA leakage from the nucleus is a sign of compromised genome stability. Using the same TGCT tissue samples we observed increased number of cells positive for dsDNA, concentrated together with STING in the cytoplasm (Fig. 3h, i). Taken together, we show upregulated immune response in leukocytes of DSD and TGCT-individuals with specific DDR-relevant stimulation in their gonads with GCT.

Autophagy is inhibited in leukocytes of DSD-individuals

Autophagy is known to be deregulated upon genomic instability. We showed accumulation of autophagy-specific proteome in leukocytes of DSD-individuals (Fig. 4a; Supplementary dataset 4). Generally, individuals with CAIS show less accumulation and even some decrease of autophagy-specific proteome, which is consistent with the absent DNA damage phenotype in these samples. To understand whether it is caused by inhibited protein degradation or stimulated protein production, we analyzed transcription of autophagy markers *LC3* and *P62* in leukocytes, and observed statistically significant decrease by two folds in *LC3* transcripts DSD-GCT and TGCT-samples (Fig. 4b–e). Later stages of autophagy require fusion with lysosome for proteolysis, and we did not detect significant downregulation in lysosomal-specific gene expression in both GCT-groups, but rather *CTSB* increase in DSD-GCTs when compared to control or Swyer and CAIS-individuals (Extended data Fig. 2d–g). These gene expression data indicate autophagy regulation on the early stages at least partially on the transcriptional level in samples with DSD and GCT.

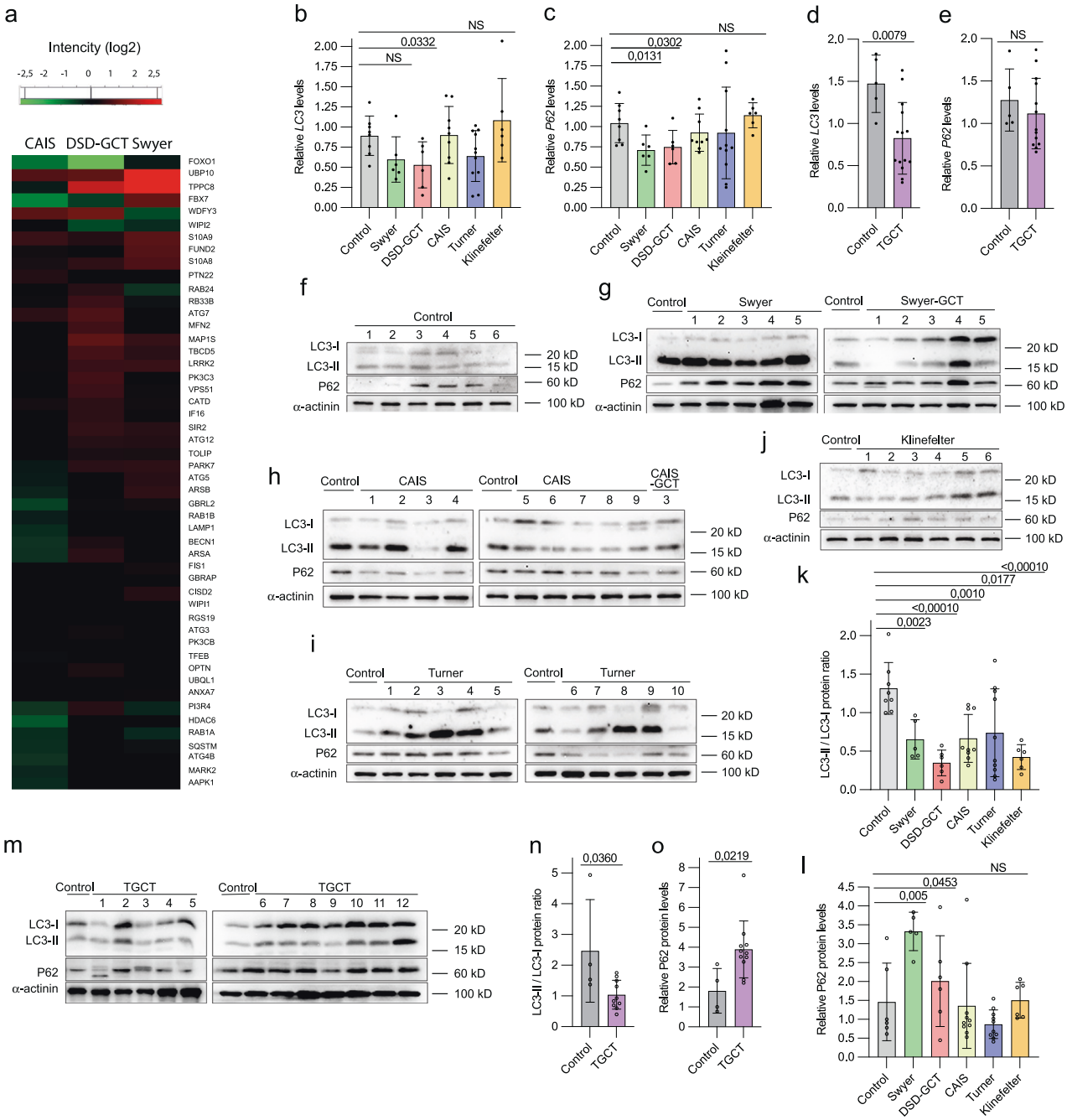

Fig. 4 Autophagy deregulation in DSD and TGCT-leukocytes samples. (**a**) Heat map of GO selection of autophagy-specific proteins from entire proteome mass spectrometry data. qRT-PCR analysis of autophagy markers *LC3* and *P63* in individuals with DSD (**b, c**) and TGCT (**d, e**). Immunoblotting for LC3 and P62 proteins for controls (**f**), Swyer and Swyer-GCT (**g**), CAIS and CAIS-GCT (**h**), Turner (**i**), Klinefelter (**j**). Quantification of the ratio of LC3-II to LC3-I (**k**) and P62 relative protein levels normalized to α-actinin (**l**) in DSD-individuals. Immunoblotting of autophagy markers for TGCT group (**m**) and quantification (**n**, **o**). Unpaired t test was used for statistical analysis, *p* values are indicated.

We analyzed protein content via measuring the ratio of active lipidated LC3-II vs. non-lipidated LC3-I protein forms. We observed in general for individuals with DSD a downregulation of LC3-II / LC3-I ratio (Fig. 4f–k). Another autophagy marker, ubiquitin-ligase P62, is normally accumulated, when its protein targets are unable to undergo autophagic degradation [39]. Accordingly, DSD-samples did not show signs of enhanced P62 protein degradation, but rather an accumulation in DSD-GCT and Swyer groups over two-folds (Fig. 4f–j, l). TGCT-samples confirmed these observations, illustrating inhibited LC3-II / CL3-I ratio and accumulation of P62 protein (Fig. 4m–o). This indicates an inhibition of autophagy flux and consequent accumulation of proteins in leukocytes of individuals with DSD and TGCT.

Therefore, we show that deregulated autophagy and type I interferon signaling supplement DNA damage phenotype in individuals with DSD.

DNA repair mechanisms are altered in leukocytes of DSD-individuals

Deficiency in DNA repair is a leading cause of genetic instability. To understand whether it is relevant to pathology in individuals with DSD we analyzed the expression of TP53, a key regulator of DNA

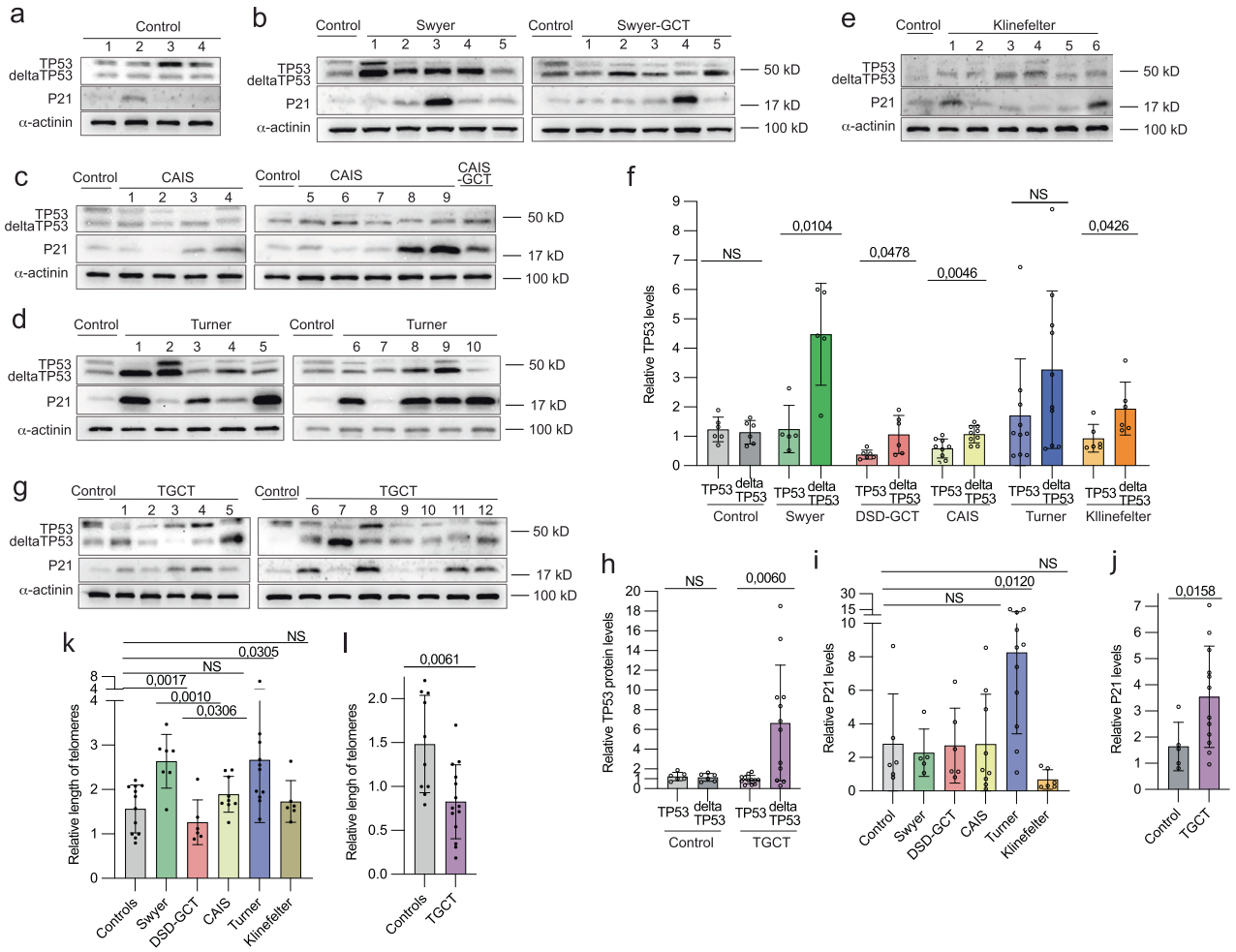

Fig. 5 Expression of TP53 protein in leukocytes of DSD- and TGCT-individuals. Immunoblotting for TP53 and P21 proteins for controls (**a**), Swyer and Swyer-GCT (**b**), CAIS and CAIS-GCT (**c**), Turner (**d**) and Klinefelter (**e**) individuals. (**f**) Relative quantification full-length (TP53) and depleted isoform (deltaTP53) of TP53 in DSD-groups. Immunoblotting (**g**) and relative quantification normalized to α-actinin (**h**) for TGCT-group. Relative quantification of P21 protein in DSD (**i**) and TGCT (**j**) groups. Quantification of relative length of telomeres in DSD (**k**) and TGCT (**l**) samples.

damage control [40]. We observed altered expressions of two TP53 protein variants: full-length (TP53) and its shorter isoform (deltaTP53). We illustrated increase in deltaTP53 expression in all DSD-samples when compared with TP53 (Fig. 5a–f), except for leukocytes from Turner-individuals that, however, showed statistically significant deltaTP53 upregulation when compared to control (Extended data Fig. 3a). The DSD-GCT group failed to upregulate deltaTP53 by four times as it was observed in Swyer, rather resembling relatively small changes in CAIS group in a context of absent DNA damage (Fig. 5f). Interestingly, TP53 was decreased in leukocytes of DSD-GCT and CAIS-individuals (Extended data Fig. 3a). DeltaTP53 positively correlates with increasing DNA damage in Swyer and Turner samples defined by γH2AX (Extended data Fig. 3b, c). In turn, low deltaTP53 protein levels in DSD-GCT-samples did not correlate with increasing DNA damage, indicating possible failure of DDR (Extended data Fig. 3b). Similarly, leukocytes of TGCT-individuals showed six-folds increase in deltaTP53, while it failed to correlate with γH2AX (Fig. 5g, h, Extended data Fig. 3d). It possibly illustrates that in some TGCT-cases with high DNA damage deltaTP53 fails to be upregulated similarly to DSD-GCT samples. Therefore, elevated expression of deltaTP53 is intrinsic to DSD-samples with genomic instability.

To better understand the consequences of TP53 protein expression alteration, we examined P21, a TP53 target gene and a key regulator of check-points. We did not detect steady upregulation of P21 among DSD-samples with increased deltaTP53, except for Turner (Fig. 5a–e, i). However, in TGCT-individuals P21 was high, reflecting accumulation of deltaTP53 (Fig. 5g, j) and p-ATM-S1981 another relevant marker of active DDR (Extended data Fig. 3e). Discrepancy in behavior of deltaTP53 and P21 may indicate a presence of alternative DDR mechanisms in Swyer individuals, restricting check-points stimulation upon DNA damage.

To additionally characterize DDR mechanisms, we analyzed the length of telomere repeats in different study groups. Deteriorating telomeres can be triggered by aberrant DNA damage repair contributing to genomic instability [41]. We observed doubled telomere length in Swyer and Turner, implying the presence of efficient DNA damage repair mechanisms, which were compromised in DSD-GCT group exposing shortened telomeres (Fig. 5k). Consistently Klinefelter and CAIS groups, with low deltaTP53, did not show an increase in telomeres length. Similar inhibition in telomere length was confirmed in TGCT leukocytes, potentially reflecting distinct status of deltaTP53 in this study group (Fig. 5l).

Taken together we showed deregulated DNA repair mechanisms in leukocytes of DSD samples. Therefore, altered TP53 protein expression may underlie their propensity for GCT development.

TP53 transactivation domain is mutated in DSD-individuals with GCT

GCT do not typically carry mutations in TP53 [42, 43]. The situation may be different in peripheral blood of study individuals. To

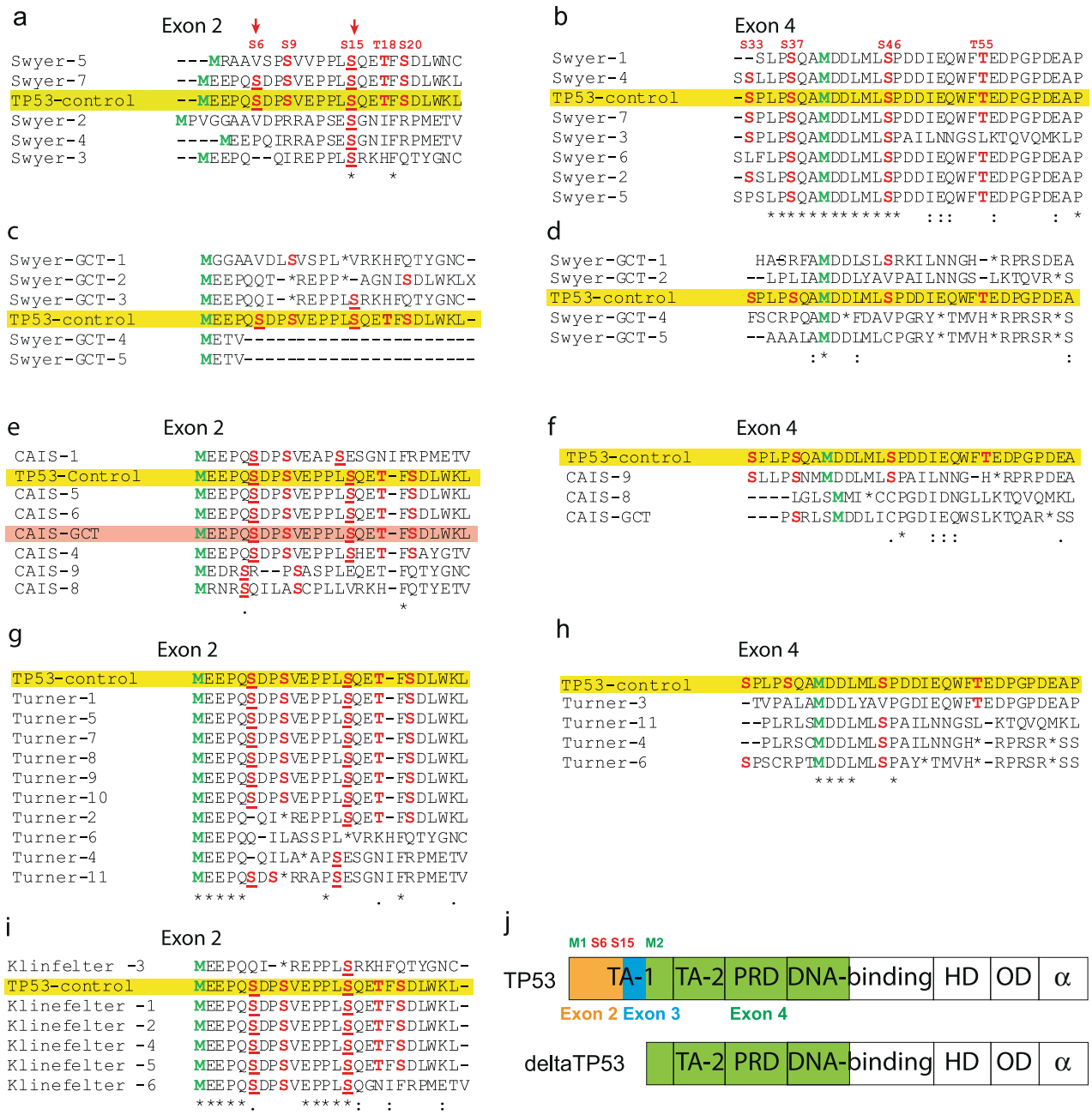

Fig. 6 Sequencing of the N-terminus of TP53 gene. Protein sequencing corresponding to transactivation domains were generated based on the DNA sequencing of exons 2 and 4. Protein sequencing of the regions encoded on exon 2 and 4 of Swyer (**a**, **b**), Swyer-GCT (**c**, **d**), CAIS and CAIS-GCT (**e**, **f**), Turner (**g**, **h**) and Klinefelter (**i**) groups. Yellow labels control sample. (**j**) Scheme illustrating depleted isoform deltaTP53 and a full-length TP53 protein.

understand the reason behind the low TP53 levels in DSD-individuals with GCT, we decided to investigate two transactivation domains (TAD) located on the N-terminus. First TAD is encoded on exons 2 and 3 that typically present in full-length TP53. However, when N-terminus is deleted, deltaTP53 only carries second TAD encoded on exon 4. TAD caries crucial Serine (S)/Threonine (T) residues that when phosphorylated block MDM2-dependent degradation of TP53 and promote its binding with other transcriptional factors [44]. The primary phosphorylation events on S6 and S15 permit consequent post-translational modifications of TP53. In the absence of this phosphorylation TP53 is prone to degradation. Sequencing of the N-terminus of TP53 gene showed missense mutations leading to a frameshift in exon 2 of individuals with Swyer and, therefore, resulting in loss of S/T residues (Supplementary dataset 5). Only two out of seven studied individuals carried both S6 and S15 similar to the control (Fig. 6a) while exon 4 was mainly unaffected (Fig. 6b), supporting an observation on stabilized deltaTP53 in individuals with Swyer (Fig. 5b, f). In turn Swyer-GCT samples had significantly altered sequences of both exons 2 and 4, which could be the reason for decreased stability and so expression of TP53 and deltaTP53 proteins, compared to Swyer without GCT (Fig. 6c, d, Fig. 5b, f). C-terminus modifications can also influence TP53 protein stability, while we detected no variability in sequences of exons 10 and 11 in Swyer samples, even with GCT (Extended data Fig. 4). Therefore, we added an analysis of exons 2 and 4 in other study groups. TAD sequences in exons 2 and 4 mainly remained unaltered in CAIS samples (Fig. 6e, f). The only exceptions with less S/T in exon 4

were samples CAIS-GCT and CAIS-8, showing hyperplastic Leydig cells by histological analysis (Fig. 6f, Extended data table 1). Turner individuals, characterized by low GCT risk, as a rule preserved critical S6 or S15 in exon 2 (Fig. 6g), with couple exceptions that contain S/T on exon 4 and, therefore, are potentially capable to stabilize the protein (Fig. 6h). Klinefelter-samples had most of the sequences similar to control (Fig. 6i). Therefore, individuals with Swyer with high risk of GCT show evidence of altered TAD sequences in TP53 which correlated with low deltaTP53 expression. While samples of CAIS, Turner and Klinefelter individuals without high GCT risk had sequences close to control and, even if TAD on exon 2 altered, it's usually backed up by unchanged TAD on exon 4 (Fig. 6j). However, it worth to mention that due to the increased TP53 mutagenesis, especially in Swyer samples, it is difficult to predict the function of the protein, whether TP53 behaves as a tumor suppressor or as an oncogene in individuals with DSD.

Rescue of genomic instability in DSD-individuals

We applied specific drugs to a primary culture of blood from individuals of DSD-GCT group in order to diminish DNA damage. Incubation was for one hour to avoid undesired influence of artificial conditions. First, in order to identify whether decreased autophagy is beneficial for DSD-phenotypes, we supplemented culture medium with Bafilomycin A1, an inhibitor of lysosomal acidity that blocks autophagy at proteolysis stage. As expected, we observed low accumulation of LC3 in DSD-GCT-samples, as an evidence of decreased autophagy flux compare to control (Fig. 7a, b). γH2AX levels were downregulated upon Bafilomycin A1 (Baf A1) addition, implying a necessity of low autophagy rates for DNA repair (Fig. 7a, c). Second, we used enoxacin, known to stimulate DDR and DNA repair via TP53, also in a context of dysfunctional telomeres [45], which successfully diminished DNA damage in DSD-GCT-leukocytes by two-folds (Fig. 7a, c). Third, we added Idasanutlin, an inhibitor of TP53 and MDM2 interaction, leading to full-length TP53 stabilization (Fig. 7a, d). However, Idasanutlin failed to rescue DNA damage (Fig. 7a, c). This potentially supports our previous observations on the relevance of deltaTP53 in DNA repair mechanisms in individuals with DSD.

To explore long-term effects of autophagy inhibition we derived lymphoblastoid cell lines from leukocytes of four DSD-individuals and fertile controls. We exposed these cells to BafA1 up to four days in culture to inhibit autophagy flux (Fig. 7e, f). We discovered that the cells could benefit from protein degradation blockade and showed an increase of their telomeres' length, which was not the case in control cell lines (Fig. 7g). In support of our previous findings on TP53 involvement in DDR regulation, we described a steady accumulation of deltaTP53 upon autophagy inhibition in DSD-samples when control cells showed decrease in relative deltaTP53 protein levels with increasing time of BafA1 treatment (Fig. 7e, h). In turn, total TP53 levels were slightly upregulated independently on BafA1 treatment conditions (Fig. 7e, i).

To summarize, we showed that rescue of DNA damage, as well as telomeres length regulation, in leukocytes of individuals with DSD can be potentially done via autophagy and by direct influence on DDR (Fig. 7j).

DISCUSSION

In our work we described an increase of DNA damage in leukocytes and gonads of DSD-individuals. We also associated DNA damage upregulation with malignancy in dysgenic gonads in different study groups, including men with TGCT by evaluating innate immune response activation. Compromised genomic DNA quality suggested an involvement of DNA repair pathways, which we illustrated by alternative TP53 protein expression and gene sequence in DSD-samples with increased DNA damage. Accordingly, telomere length was upregulated in parallel with increased deltaTP53 expression, suggesting active DNA repair mechanisms in Swyer and Turner individuals, while both were decreased in GCT-group. TP53 exhibited a significant increase in missense mutations in a region, encoding transactivation domains and, therefore, potentially compromises protein stability. We also illustrated that leukocytes of DSD-individuals are responsive to chemicals regulators, diminishing DNA damage upon direct DNA repair mechanisms activation or autophagy inhibition.

Given that genetic causes for DSD remain unknown for about half of the patients, it's likely that polygenic mutations or even noncoding regions of genome could be involved [46]. This supports our idea that a state of genome integrity is behind DSD-phenotypes. DSD-individuals often show signs of unstable genome, such as genetic mosaicism with highly variable phenotypes, caused by differences in Y-chromosome breakpoints, unstable idic(Y) chromosomes or dynamic distribution of mosaicism through the organism [47]. Accordingly, we described Swyer and Turner individuals carrying high DNA damage and altered TP53 protein expression that could explain functional or total loss of Y chromosome. Genomic instability in blood of these individuals seems to be associated with gonadal dysgenesis. Accordingly, CAIS, caused by mutated androgen receptor, does not have signs of DNA damage, and sometimes is associated with residual germ cells in relatively well-developed gonads. In turn, DNA damage in men with Klinefelter is likely due to the extra chromosome presence [25]. Phenotypically males with Klinefelter syndrome possess compromised fertility, however, in some cases gonads have residual spermatogenesis, illustrating the presence of functional Y chromosomes.

The critical role of genome integrity has been already discussed for germ cells and embryogenesis in humans [48]. Our data imply a possibility that genotoxic stress in individuals with Swyer or Turner may already be present at the moment of sex tissue determination and, therefore, could potentially interfere with gonadal formation due to the defective gene expression from unstable sex chromosomes. Indeed, we observed signs of genome deterioration in misshaped nuclei of cells [37] of so-called streak gonads of Swyer and Turner individuals, while this phenotype was less pronounced in CAIS testicle-like gonads. Genomic instability has been already described in GCT cells of individuals diagnosed with CAIS, however, it was associated with mobility of transposable elements [49]. Considering our findings on the increased load of DSBs in the blood of individuals with DSD, we propose that the state of deterioration of genome integrity likely goes above the transposons activity and could be a consequence of the general misfunction of DNA repair.

TP53 with its high genetic polymorphism is the most commonly mutated gene in cancers [50]. Full-length protein is known to regulate DDR and being stimulated via N-terminus TAD [51]. We described a repetitive loss of critical serine residues on N-terminus of TP53 and demonstrated a decrease of TP53 protein in individuals with DSD. In turn, deltaTP53 is associated with high DNA damage in individuals with Swyer and Turner without GCT. Failing to upregulate deltaTP53 seems to potentially increase susceptibility to GCT development in DSD-group. It was shown that suppressed TP53 function causes insensitivity to DDR and continuous cell proliferation, leading to severe shortening of telomeres that normally happens during senescence [52, 53]. This could be the reason for decreased telomere length in leukocytes from DSD-GCT group when compared to individuals with Swyer and CAIS without GCT. The situation in TGCT was even more evident with shortened telomeres below the controls' level. Shortened uncapped telomeres tend to fuse, which is accompanied by a whole bunch of genomic instability phenotypes: increased DSBs, chromosomal aneuploidy, micronuclei, misshaped nucleus, chromatin bridges [54]. In our work we described some of these signs of genotoxic stress in leukocytes and dysgenic gonads, which correlates with TP53 mutation phenotypes.

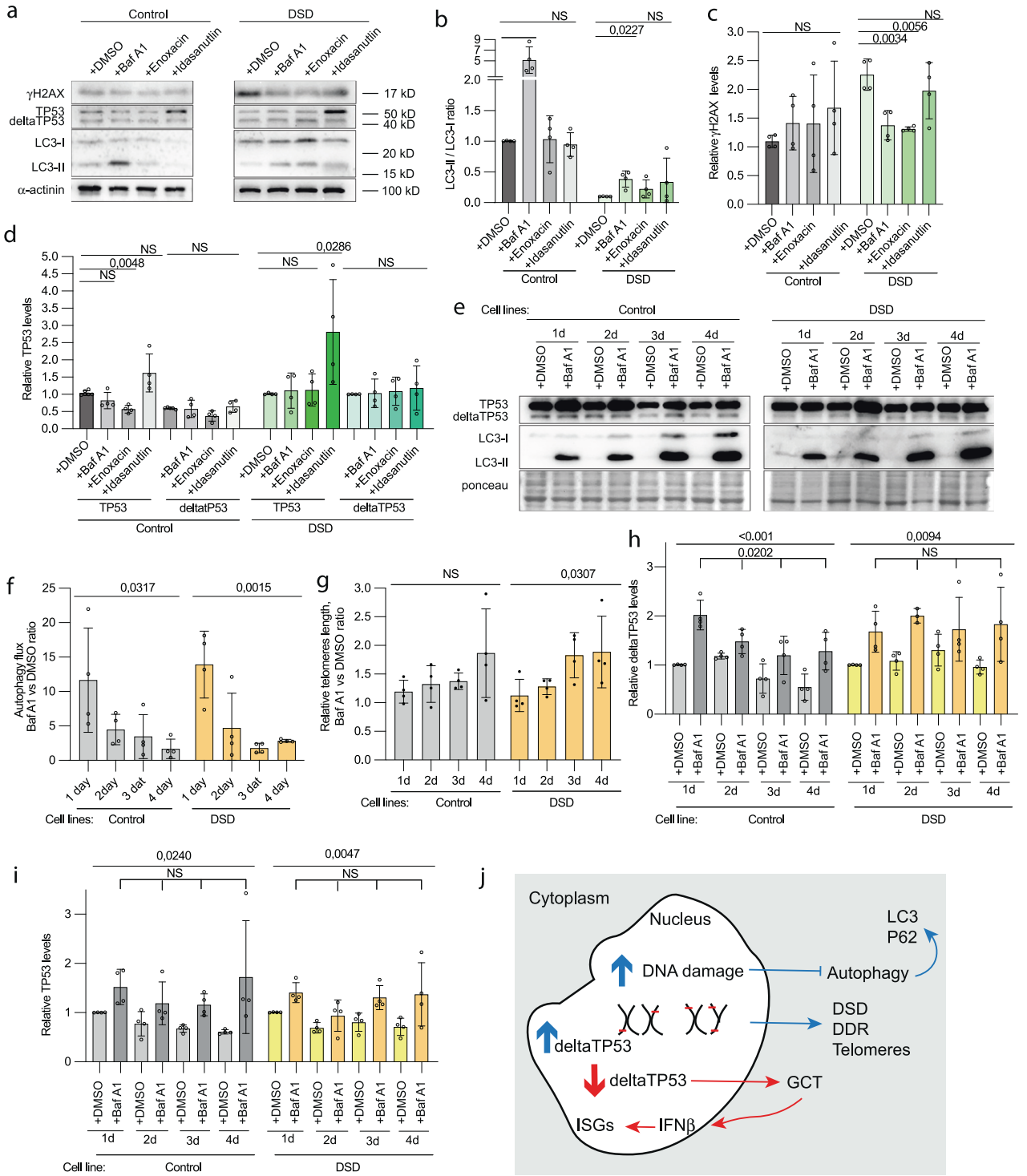

Fig. 7 Effects on DNA damage and DDR after short-term culture with drugs. a Immunoblotting for TP53, γH2AX and LC3 of control and DSD-samples cultured with Bafilomycin A1 (Baf A1), Enoxacin, Idasanutlin. α-actinin was used as a loading control. (**b**) Quantification of the ratio of LC3-II vs LC3-I of the immunoblotting (**a**). Relative protein levels of γH2AX (**c**) and TP53 (**d**). **e** Immunoblotting representing TP53, LC3 and loading control ponceau of samples from DSD-individuals and control lymphoblastoid cell lines treated with 100 μM BafA1. **f** Relative quantification of autophagy flux based on LC3 protein expression on the immunoblotting (**e**). **g** Relative telomere length changes upon autophagy inhibition. Relative quantification of protein levels normalized to ponceau for deltaTP53 (**h**) and total TP53 (**i**) levels from immunoblotting (**e**). **j** A summary scheme illustrating phenotypes specific for DSD (blue arrows) and GCT (red arrows).

Turner and Swyer both have increased deltaTP53, however, only Turner showed P21 induction. This could be dependent from upregulated TP53 in Turner, while there's different situation in Swyer group, possibly relying on mechanisms working against check-points activation. Accordingly, we observed increased length of telomeres in Swyer- and Turner-samples. Discrepancies between TGCT and DSD samples in deltaTP53 regulation show that TGCT samples could have variable reasons for tumor development.

Steady P21 upregulation in TGCT samples also indicates on potentially functional TP53 signaling. On the other hand, the intracellular distribution of P21 could play a role in its function specification and, therefore, alternative DDR regulation [55, 56].

The cell death mechanisms in genotoxic crisis were uncovered only recently and evidently autophagy plays a key role [39]. We showed for the first time that autophagy and type I Interferon response reflect the state of genomic DNA in DSD- and TGCT-group samples. Accordingly, in leukocytes of individuals of studied groups with increased DNA damage, we observed downregulation of autophagy-specific gene expression. It is possible that low autophagy prevents apoptosis of cells experiencing genotoxic stress. Indeed, cells with compromised TP53 function and unprotected telomeres are targeted by autophagy [57]. And cells with knockout of TP53 and ATG7, a key autophagy protein, exhibit intensive proliferation and improved survival rates, since they can bypass senescence. We observed decrease in DNA damage levels in leukocytes from individuals with DSD, when autophagy was chemically blocked. It could possibly be connected to the previously described negative influence of autophagy on TP53, and so DNA repair, via proteasomal degradation [58]. It might be that artificial blockade of autophagy sustained the pull of crucial DDR players for individuals diagnosed with DSD and as a consequence positively influenced on genome status. On the other hand, TP53 promotes autophagy-specific gene expression [59], which could also possibly explain a decrease of autophagy in leukocytes of individuals with DSD susceptible to TP53 missense mutagenesis. Our data seems also to be in agreement with recently proposed immortalization models, where authors propose loss of TP53 and autophagy function for cells escaping telomere shortening crisis [57].

In addition to autophagy, innate immune response is known to be activated by an unstable genome. We observed characteristic for DSD-individuals leukocytes upregulation of immune response-related proteome with specific changes in samples from individuals with GCT. IFNβ signals are stimulated due to the leakage of genomic DNA into the cytoplasm [25]. Indeed, we detected increased presence of STING protein the key player of cGAS-STING pathways transmitting signals from cytoplasmic dsDNA to the nucleus for type I interferon response stimulation. STING also co-localized with dsDNA in cytoplasm in GCT-cells connecting phenotypes observed in peripheral blood to the actual place of tumorigenesis. In turn, deregulated expression of RNA helicases in DSD-GCT leukocytes samples implies potential downregulation of RNA-induced interferon signaling and its irrelevance from STING-dependent mechanism [60]. These findings additionally emphasize an importance to study genome stability in individuals with DSD and TGCT that have high propensity to GCT development.

Interestingly, we also observed upregulated *IFNβ* in leukocytes of individuals with CAIS, which is likely due to suppressed androgen function [61]. The role of androgen signaling in GCT regulation and how it is relevant to our study groups is another exciting direction of investigation.

In conclusion, we described increased DNA damage phenotype in individuals with differences of sex development and men with testicular germ cell tumors. We defined DDR phenotypes, including type I Interferon response and autophagy. DDR regulator TP53 was mutated in samples from individuals developing GCT, which suggests a new focus for cancer diagnostics and prophylactic treatments to facilitate DSD and GCT-relevant phenotypes.

MATERIAL AND METHODS

Patients material

Individuals with Differences of Sex Development were enrolled into study during routine praxis in the Department of Gynecology Endocrinology and Infertility Disorders. The samples from men with testicular germ cell tumors were provided us by Urology Department. The study was approved by the ethical committee and the samples were collected with written patients consent. For this study, we analyzed 40 individuals with DSD and 19 samples with GCT. DSD-individuals included individuals with Swyer, Turner, Klinefelter and Complete Androgen Insensitivity (CAIS) Syndromes. The study groups are listed with additional information (Extended data table 1 and 3). The sample undergo standard characterization procedure in genetics and histological facility of Heidelberg University Hospital. The control group contain samples from fertile men and women (Extended data table 2).

Leukocytes isolation from the peripheral blood

Blood was collected in EDTA and subjected to leukocytes isolation according to the stablished protocol. 10 ml of blood was mixed with 30 ml of lysis buffer (155 mM NH_4Cl, 10 mM KHCO3, 0,1 mM EDTA ph 7.4) and incubated 30′ on ice. Then mix was centrifuged 10′ at 1200 rpm at 4 °C. The pellet was washed three times with 10 ml lysis buffer and then subjected for DNA, RNA and protein isolation with NucleoSpin® TriPrep kit (Marcherey-Nagel).

EBV-transformed lymphoblastoid cells

EBV stock was prepared from cultures of EBV-transformed marmoset cells, strain B95-8. The B95-8′ strain of EBV was used to transform human B lymphocytes as it was previously described [62]. 10 ml EDTA-blood was mixed with 30 ml of Lysis buffer (155 mM NH_4Cl, 10 mM KHCO3, 0,1 mM EDTA ph 7.4) and left for 30′ on ice, then centrifuged for 10′ at 1200 rpm and 4 °C. The pellet was washed three times with 10 ml of of Lysis buffer and resuspended with 3 ml of culture medium, containing RPMI Medium 1640 (with stable L-Glutamin) Cat.# 61870010, ThermoFisher Scientific) plus 10% FBS (Cat.# 10500064, ThermoFisher Scientific), penicillin (50 U/ml), streptomycin (25 pg/ml) (Cat.# 15140122, ThermoFisher Scientific), gentamycin (Cat.# 15710, ThermoFisher Scientific), NEA (Cat.# 11140035, ThermoFisher Scientific) and sodium pyruvate (Cat.# 11360070, ThermoFisher Scientific). After virus stock was added at 1 /10 final dilution to a cell suspension containing $2 \times l0^6$ cells/ml. The virus was allowed to adsorb to the cells for 2 h at 37 °C. Cells were then pelleted by low-speed centrifugation and resuspended at 2×10^6 cells/ml in culture medium.

The cell lines of four DSD-individuals (three Turner and one Swyer syndrome) and controls (two males and two females) were culture with 100 µM Bafilomycin A1 for 1, 2, 3 and 4 days, DMSO was used as a control.

Mass spectrometry

Proteome-wide expression profiling of leukocytes from three Swyer (Extended data table 1, samples 1, 2, 8), three CAIS (Extended data table 1, samples 2, 4, 7), three DSD-GCT (Extended data table 1, samples 1, 2, 4) individuals and three fertile controls (Extended data table 2, samples 1, 2, 8), was supported by the Core Facility for Mass Spectrometry & Proteomics (CFMP) at the Center for Molecular Biology at University Heidelberg (ZMBH). 50 µg of protein was precipitated using Wessel-Flügge method [63] and protein pellet was dissolved in 8 M Urea buffer. After reduction and alkylation for 30 min at RT using 10 mM TCEP and 40 mM CAA, Lys-C was added at 1:100 enzyme:protein ratio and incubated for 4 h at 37 °C. Mixture was diluted 1:4 with 50 mM TEAB pH 8.5 and trypsin was added in ratio 1:50. After overnight incubation at 37 °C, samples were acidified, desalted on self-made C18 Empore® extraction discs (3 M) StageTips [64], concentrated in a SpeedVac and stored at −20 °C until measured.

Samples were suspended in 0.1% TFA and an equivalent to 1 µg of peptides was analyzed using Ultimate 3000 liquid chromatography system coupled to an Orbitrap QE HF (Thermo Fisher). An in-house packed analytical column (75 µm x 200 mm, 1.9 µm ReprosilPur-AQ 120 C18 material Dr. Maisch, Germany) was used. Mobile phase solutions were prepared as follows, solvent A: 0.1% formic acid / 1% acetonitrile, solvent B: 0.1% formic acid, 89.9% acetonitrile.

Peptides were separated in a 120 min linear gradient started from 3% B and increased to 23% B over 100 min and to 38% B over 20 min, followed by washout with 95% B. The mass spectrometer was operated in data-dependent acquisition mode, automatically switching between MS and MS2. MS spectra (m/z 400–1600) were acquired in the Orbitrap at 60,000 (m/z 400) resolution and MS2 spectra were generated for up to 15 precursors with normalized collision energy of 27 and isolation width of 1.4 m/z.

The MS/MS spectra were searched against the Swiss-Prot Homo sapiens protein database (UP000005640, June 2020, 20531 sequences) and a customized contaminant database (part of MaxQuant, MPI Martinsried) using Proteome Discoverer 2.5 with Sequest HT (Thermo Fisher Scientific). A fragment ion mass tolerance was set to 0.02 Da and a parent ion mass tolerance to 10 ppm. Trypsin was specified as enzyme. Carbamidomethyl was set as fixed modification of cysteine and oxidation (methionine),

acetylation (protein N-terminus) and methionine loss (protein N-terminus) as variable modifications. Peptide quantification was done using precursor ion quantifier node with Top N Average method set for protein abundance calculation and N for Top N set to 3.

For comparison of each DSD group with the control we calculated the protein levels fold change ratios. The same datasets were used to analyze DDR, autophagy- and immune response, and P53-specific proteome. Presence of at least one unique peptide is required for the identification of reported protein groups. Minimum of two ratio counts were required for the quantitation based only on unique and razor peptides. Differential expression of proteins was defined by T-test (FDR q-values calculated with Perseus) and used for log2 intensities of samples from DSD-groups, normalized to control (Supplementary datasets 1–4).

The proteomics data used in this manuscript are deposited in the ProteomeXchange Consortium (http://proteomecentral.proteomexchange.org) via the PRIDE partner repository and can be accessed with a code PXD033635.

Sequencing

We used genomic DNA of individuals with DSD for sequencing. We analyzed exons 2-3 and exon 4 of P53 gene according to the established protocol (IARC, 2019). The primers used for exons 2-3 F-tctcatgctggatccccact; R-agtcagaggaccaggtcctc; exon 4 F-tgctcttttcacccatctac; R-atacggccaggcattgaagt. The sequencing was performed using BigDye Terminator v1.1 Cycle Sequencing Kit (Applied Biosystems, Cat. no. 4337450) and the ABI PRISM 3100 Genetic Analyzer. Sequencing Data that support the findings of this study have been deposited into open access NCBI GeneBank with the accession codes for ON398074 - ON398077, ON398079 - ON398085, ON398088 - ON398090, ON398092 - ON398110 (TP53-exon2) and ON398111 - ON398128 (TP53-exon4). Sequence results from forward and reverse primers were considered for the evaluation of real variants to avoid technical errors. DNA alignments to reference TP53 sequence are presented (Supplementary dataset 5).

Western blotting

Protein from leukocytes was analyzed via Western Blot analysis following modified protocol [65]. The protein concentration was determined by Protein Quantification Assay (Cat.# 740967,Macherey-Nagel). 10 µg of the protein was separated by SDS-PAGE electrophoresis, then transferred onto PVDF membrane (Immobilon-P membrane (Cat.# IPVH00010, Millipore). The membrane was blocked with 5% skim milk (Cat. # T145, Carl Roth) or 3 % BSA (Cat. # 8076.4, Carl Roth) 1 h at RT. Then incubated at 4 °C overnight with primary antibodies. After washing three times with buffer TNT (50 mM Tris, 150 mM NaCl, 5 mM EDTA and 0.05% Tween 20; pH 7.6), the membrane was incubated with corresponding secondary antibodies (peroxidase conjugated Goat Anti-Rabbit IgG (Cat.# 111-035-046, Dianova) or peroxidase-conjugated Goat Anti-Mouse IgG (Cat.# 115-035-062, Dianova) for 1 h at RT. Protein bands were visualized by enhanced chemiluminescence with an ECL kit (SuperSignal West Femto Substrat (Cat. # 34095, Thermo Scientific). Image development was performed on iBright FL1000 Imager (Cat.# A32748, Invitrogen). Antibodies list is provided (Extended data table 4). Every point in the plots of data for WB analysis represents one individual patient sample or experimental measurement, total sample size is represented by 3-10 points on the graph. The means of each measurement/experiment were calculated and plotted for presentation and for statistical analysis using GraphPad. Two-sided unpaired t test was used, and p-values, s.d. and error bars are shown on the graphs. Original data files are presented (Supplementary file 6).

Quantitative real-time PCR

1 µg RNA was used for cDNA synthesis with Superscript II (Cat.# 18064022, Invitrogen). qPCR analysis was performed on an ABI Prism 7900HT Fast Real-Time PCR System (Applied Biosystems). The cycling conditions were as follows: 50 °C for 2 min, denaturation at 95 °C for 10 min followed by 40 cycles at 95 °C for 15 s, and a combined annealing and extension step at 60 °C for 60 s. The list of TaqMan assays (Termofisher) is provided (Extended data table 5). Every point in the plots of data for qRT-PCR analysis represents one individual patient sample or experimental measurement, total sample size is represented by 3-10 points on the graph. The means of each measurement/experiment were calculated and plotted for presentation and for statistical analysis using GraphPad. Two-sided unpaired t test was used, and p-values, s.d. and error bars are shown on the graphs. No RT control were used.

Blood culture with drugs

For each condition we prepared 10 cm dishes with 10 ml culture medium, containing 2 ml of blood, collected in citrate and containing approximately 5×10^6 leukocytes per 1 ml; 15% FCS (Cat. #10500064, Life Technologies); 20 µl PHA-L (Cat.# 00-4977-03, Life Technologies). We added Enoxacin (10 µM, S1756, Selleckchem), Idasanutlin (10 µM, HY-15676, Hycultec), Bafilomycin A1 (100 nM, 11038, Cayman). DMSO was used as the control. After 1 h incubation at 37 °C, 5%CO2 cells were collected, washed 2 times with 1xPBS (Cat. # 14190-094, Gibco) and subjected to leukocytes isolation procedure as described above. DNA, RNA and protein isolation from the leukocytes was performed with NucleoSpin® TriPrep kit (Marcherey-Nagel). The experiment was executed four times.

Hematoxylin/eosin staining and microscopy

Tissue biopsies were fixed in buffered formaldehyde and subsequently embedded in paraffin. Sections, 4 µm thick, were stained with the standard protocol for Hematoxylin / Eosin. Immunohistochemistry for AMH was performed as previously published [12]. The imaging was performed using light microscope (LEICA) with magnification 100x. The image analysis was performed using ImageJ software. The circularity and roundness parameters were plotted for statistical analysis using GraphPad.

Immunofluorescence

Immunostaining was performed on 4 µm dehydrated FFPE tissue sections. Antigen retrieval was performed by immersing the slides in 10 mM citrate buffer (pH 6.0) in a steamer for 10 min. Next, tissue sections were allowed to cool and then kept at room temperature for 20 min. Slides were washed twice in PBS and three times in washing buffer (PBS containing 0,1 % Triton X-100). Tissue sections were incubated in 3% H_2O_2/Methanol for 10 min. Sections were washed three times with washing buffer and then blocked with blocking buffer (5% goat serum (cat. # S-1000, Vector) in washing buffer) for 1 h at room temperature. Tissue sections were incubated with the primary antibody in a humid box at 4 °C for 16 h. The primary was diluted in 1% goat serum/washing buffer. After three washes in washing buffer secondary fluorescence-conjugated antibodies (Goat Anti-Rabbit/Mouse DyLight 488 conjugated, cat # 35552, Thermo Scientific) was diluted to a concentration of 2 µg/ml in 1% goat serum/washing buffer and incubated for 2 h at room temperature in a dark humid box. Slides were then rinsed in washing buffer five times for 3 min each and nuclei were stained with 4′,6-diamidino-2-phenylindole (DAPI, cat # D-1388, Sigma) at a concentration of 1 µg/ml for 10 min at RT. Sections were then rinsed three times with water for 3 min each before being mounted and coverslips were applied using ProLong Glass Antifade Mountant (cat. #P36980, Invitrogen). The imaging was performed using a fluorescence microscope (LEICA, DMLB), using a HQ camera SpectraCube (Applied Spectral Imaging, Mannheim, Germany) and a 20x-air, 63x-oil or 100x-oil objective (PL FLUOTAR 20x/0,5 PH2, HCX PL APO 63x/1,32-0,6 OIL, PL FLUOTAR 100x/1,3 OIL PH3) under the control of the Spectral imaging acquisition software 2.6 (Applied Spectral Imaging, Germany). For immunofluorescent analysis, 100–1000 s of cells were analyzed using the automatic software ImageJ. The means of each measurement/experiment were calculated and plotted for presentation and for statistical analysis using GraphPad. Two-sided unpaired t test was used, and p-values, s.d. and error bars are shown on the graphs.

Primary antibodies used anti-γ-H2AX rabbit polyclonal antibody (0,25 µg/mL, cat.#ab11174, Abcam), anti-STING (D2P2F) rabbit monoclonal (1/50 dilution, 13647 S, Cell Signaling Technology), anti-dsDNA mouse monoclonal (1/50 dilution, 58749, Santa Cruz Biotechnology), anti-OCT4 mouse monoclonal (1/300 dilution, cat.#SC-5279, Santa Cruz Biotechnology).

Gonadal tissue sections were provided by the tissue bank of the National Centre for Tumor Diseases (NCT, Heidelberg, Germany) in accordance with the regulations of the tissue bank and the approval of the ethics committee of Heidelberg University.

Telomere length assay

Genomic DNA was isolated from blood according the previously established protocol. In short, 10 ml of blood collected in EDTA was mixed with 30 ml of lysis buffer (155 mM NH_4Cl, 10 mM KHCO3, 0,1 mM EDTA pH7.4), incubated on ice for 30′ and centrifuged for 10′ at 1200 rpm, 4 °C. The pellet was washed three times with 10 ml of lysis buffer and resuspended in 5 ml of SE-Buffer (75 mM NaCl, 25 mM EDTA pH 8.0), supplemented with 250 µl of 20% SDS and 40 µl Proteinase K (10 mg/ml) and left overnight at 37 °C. Salt precipitation was done by repetitive mix

with 15 ml with SE-Buffer, supplemented with 3,3 ml of saturated NaCl and centrifugation for 15′ at RT until complete removal of the pellet. Next, DNA precipitation was performed with 1,7 ml 3 M Sodium-Acetat pH7.0 and 17 ml Isopropanol. After DNA-fiber could be collected, wash them with 80% Ethanol. Let the fiber dry and dissolve them in TE (10 mM Tris, 1 mM EDTA pH 8.0). We used 5 µg of genomic DNA per reaction for Relative Human Telomere Length Quantification qPCR Assay Kit (Cat. #8908, ScienCell). Every point in the plots of data for qRT-PCR analysis represents one individual patient sample, total sample size is represented by 3–10 points on the graph.

DATA AVAILABILITY

Mass spectrometry and sequencing data were deposited in to the open access databases, which is noted in the Material and Methods section. The other data are available upon request from the corresponding author.

REFERENCES

1. Capel B. Vertebrate sex determination: evolutionary plasticity of a fundamental switch. Nature Publishing Group 2017;18. https://doi.org/10.1038/nrg.2017.60.
2. Colaco S, Modi D. Genetics of the human Y chromosome and its association with male infertility. Reprod Biol Endocrinol. 2018;16:1–24.
3. Teitz LS, Pyntikova T, Skaletsky H, Page DC. Selection Has Countered High Mutability to Preserve the Ancestral Copy Number of Y Chromosome Amplicons in Diverse Human Lineages. Am J Hum Genet. 2018;103:261–275.
4. Ly P, Teitz LS, Kim DH, Shoshani O, Skaletsky H, Fachinetti D, et al. Selective y centromere inactivation triggers chromosome shattering in micronuclei and repair by non-homologous end joining. Nat Cell Biol. 2017;19:68–75.
5. Corujo D, Buschbeck M. Post-translational modifications of H2A histone variants and their role in cancer. Cancers (Basel). 2018;10. https://doi.org/10.3390/cancers10030059.
6. Burma S, Chen BP, Murphy M, Kurimasa A, Chen DJ. ATM Phosphorylates Histone H2AX in Response to DNA Double-strand Breaks. J Biol Chem. 2001;276:42462–7.
7. Ford CE, Jones KW, Polani PE, De Almeida JC, Briggs JH. A Sex-Chromosome Anomaly In A Case of Gonadal Dysgenesis (Turner's Syndrome). Lancet. 1959;273:711–3.
8. Jacobs PA, Strong JA. A case of human intersexuality having a possible XXY sex-determining mechanism. Nature. 1959;183:302–3.
9. Sinclair AH, Berta P, Palmer MS, Hawkins JR, Griffiths BL, Smith MJ, et al. A gene from the human sex-determining region encodes a protein with homology to a conserved DNA-binding motif. Nature. 1990;346:240–4.
10. Oosterhuis JW, Looijenga LHJ. Human germ cell tumours from a developmental perspective. Nat Rev Cancer 2019 19:9. 2019;19:522–537.
11. Ng SB, Yong MH, Knight LA, Lee VKM, Nadarajah S, Stoop H, et al. Gonadoblastoma-associated mixed germ cell tumour in 46,XY complete gonadal dysgenesis (Swyer syndrome): Analysis of Y chromosomal genotype and OCT3/4 and TSPY expression profile. Histopathology 2008;52:644–6.
12. Vogt PH, Besikoglu B, Bettendorf M, Frank-Herrmann P, Zimmer J, Bender U, et al. Gonadoblastoma y locus genes expressed in germ cells of individuals with dysgenetic gonads and a y chromosome in their karyotypes include DDX3Y and TSPY. Hum Reprod. 2019;34:770–9.
13. Cools M, Drop SLS, Wolffenbuttel KP, Oosterhuis JW, Looijenga LHJ. Germ cell tumors in the intersex gonad: Old paths, new directions, moving frontiers. Endocr Rev. 2006;27:468–484.
14. Pyle LC, Nathanson KL. A practical guide for evaluating gonadal germ cell tumor predisposition in differences of sex development. Am J Med Genet C Semin Med Genet. 2017;175:304–314.
15. Deans R, Creighton SM, Liao LM, Conway GS. Timing of gonadectomy in adult women with complete androgen insensitivity syndrome (CAIS): Patient preferences and clinical evidence. Clin Endocrinol (Oxf). 2012;76:894–8.
16. Dabrowski E, Johnson EK, Patel V, Hsu YC, Davis S, Goetsch AL, et al. Turner Syndrome with Y Chromosome: Spontaneous Thelarche, Menarche, and Risk of Malignancy. J Pediatr Adolesc Gynecol. 2020;33:10–14.
17. Oosterhuis JW, Stoop H, Honecker F, Looijenga LHJ. Why human extragonadal germ cell tumours occur in the midline of the body: Old concepts, new perspectives. Int J Androl. 2007;30:256–264.
18. Bagrodia A, Lee BH, Lee W, Cha EK, Sfakianos JP, Iyer G, et al. Genetic determinants of cisplatin resistance in patients with advanced germ cell tumors. J Clin Oncol. 2016;34:4000–7.
19. Hussong J, Crussi FG, Chou PM. Gonadoblastoma: Immunohistochemical localization of Mullerian- inhibiting substance, inhibin, WT-1, and p53. Mod Pathol. 1997;10:1101–5.
20. Deeb A, Al Suwaidi H, Attia S, Al Ameri A. 17-hydroxylase/17,20-lyase deficiency due to a R96Q mutation causing hypertension and poor breast development. *Endocrinol Diabetes Metab Case Rep* 2015;2015. https://doi.org/10.1530/edm-15-0069.
21. Gravholt CH, Dollerup OL, Duval L, Mejlgaard E, Stribolt K, Vang S, et al. A rare case of embryonal carcinoma in a patient with turner syndrome without Y chromosomal material but mutations in KIT, AKT1, and ZNF358 demonstrated using exome sequencing. Sex Dev. 2018;11:262–8.
22. Roth LM, Czernobilsky B, Mann SA, Cheng L. Gonadoblastoma versus ovarian mixed germ cell-sex cord stromal tumor in women or girls with no evidence of a disorder of sex development: A problem in differential diagnosis. Pathol Res Pract. 2020;216:153198. https://doi.org/10.1016/j.prp.2020.153198.
23. Cools M, Honecker F, Stoop H, Veltman JD, De Krijger RR, Steyerberg E, et al. Maturation delay of germ cells in fetuses with trisomy 21 results in increased risk for the development of testicular germ cell tumors. Hum Pathol. 2006;37:101–111.
24. Raznahan A, Parikshak NN, Chandran V, Blumenthal JD, Clasen LS, Alexander-Bloch AF, et al. Sex-chromosome dosage effects on gene expression in humans. Proc Natl Acad Sci USA. 2018;115:7398–7403.
25. Krivega M, Stiefel CM, Karbassi S, Andersen LL, Chunduri NK, Donnelly N et al. Genotoxic stress in constitutive trisomies induces autophagy and the innate immune response via the cGAS-STING pathway. Commun Biol. 2021;4. https://doi.org/10.1038/s42003-021-02278-9.
26. Hong DS, Reiss AL. Cognitive and neurological aspects of sex chromosome aneuploidies. Lancet Neurol. 2014;13:306–318.
27. Seminog OO, Seminog AB, Yeates D, Goldacre MJ. Associations between Klinefelter's syndrome and autoimmune diseases: English national record linkage studies. Autoimmunity. 2015;48:125–8.
28. Trolle C, Nielsen MM, Skakkebæk A, Lamy P, Vang S, Hedegaard J, et al. Widespread DNA hypomethylation and differential gene expression in Turner syndrome. Sci Rep. 2016;6:1–14.
29. Ji J, Zöller B, Sundquist J, Sundquist K. Risk of solid tumors and hematological malignancy in persons with Turner and Klinefelter syndromes: A national cohort study. Int J Cancer. 2016;139:754–8.
30. Viuff MH, Stochholm K, Lin A, Berglund A, Juul S, Gravholt CH. Cancer occurrence in Turner syndrome and the effect of sex hormone substitution therapy. Eur J Endocrinol. 2021;184:79–88.
31. Schoemaker MJ, Swerdlow AJ, Higgins CD, Wright AF, Jacobs PA. Cancer incidence in women with Turner syndrome in Great Britain: a national cohort study. Lancet Oncol. 2008;9:239–246.
32. Zhu J, Tsai HJ, Gordon MR, Li R. Cellular Stress Associated with Aneuploidy. Dev Cell. 2018;44:420–431.
33. McLaughlin M, Patin EC, Pedersen M, Wilkins A, Dillon MT, Melcher AA, et al. Inflammatory microenvironment remodelling by tumour cells after radiotherapy. Nat Rev Cancer. 2020;20:203–217.
34. Krivega M, Storchova Z. Consequences of trisomy syndromes – 21 and beyond. Trends Genet. 2022. https://doi.org/10.1016/J.TIG.2022.11.004.
35. Krivega M, Stiefel CM, Storchova Z. Consequences of chromosome gain: A new view on trisomy syndromes. Am J Hum Genet. 2022;109:2126–2140.
36. Zhang J, He Y, Shen X, Jiang D, Wang Q, Liu Q et al. γ-H2AX responds to DNA damage induced by long-term exposure to combined low-dose-rate neutron and γ-ray radiation. Mutat Res Genet Toxicol Environ Mutagen 2016;795. https://doi.org/10.1016/j.mrgentox.2015.11.004.
37. Hwang S, Williams JF, Kneissig M, Lioudyno M, Rivera I, Helguera P, et al. Suppressing Aneuploidy-Associated Phenotypes Improves the Fitness of Trisomy 21 Cells. Cell Rep. 2019;29:2473–2488.e5.
38. Alfano M, Tascini AS, Pederzoli F, Locatelli I, Nebuloni M, Giannese F et al. Aging, inflammation and DNA damage in the somatic testicular niche with idiopathic germ cell aplasia. Nat Commun 2021;12. https://doi.org/10.1038/s41467-021-25544-0.
39. Nassour J, Radford R, Correia A, Fusté JM, Schoell B, Jauch A, et al. Autophagic cell death restricts chromosomal instability during replicative crisis. Nature. 2019;565:659–663.
40. Waldman T, Kinzler KW, Vogelstein B. p2! Is Necessary for the p53-mediated G, Arrest in Human. Cancer Cells' Cancer. 1995;55:5187–5190.
41. Lazzerini-Denchi E, Sfeir A. Stop pulling my strings — what telomeres taught us about the DNA damage response. Nat Rev Mol Cell Biol 2016 17:6. 2016;17:364–378.
42. Heimdal K, Lothe RA, Lystad S, Holm R, Fosså SD, Børresen AL. No germline TP53 mutations detected in familial and bilateral testicular cancer. Genes Chromosomes Cancer. 1993;6:92–7.
43. Peng HQ, Hogg D, Malkin D, Bailey D, Gallie BL, Bulbul M, et al. Mutations of the p53 gene do not occur in testis cancer. Cancer Res. 1993;53:3574–8.
44. Appella E, Anderson CW. Post-translational modifications and activation of p53 by genotoxic stresses. Eur J Biochem. 2001;268:2764–2772.
45. Gioia U, Francia S, Cabrini M, Brambillasca S, Michelini F, Jones-Weinert CW, et al. Pharmacological boost of DNA damage response and repair by enhanced biogenesis of DNA damage response RNAs. Sci Rep. 2019;9:1–15.

46. Atlas G, Sreenivasan R, Sinclair A. Targeting the Non-Coding Genome for the Diagnosis of Disorders of Sex Development. Sex Dev. 2021;15:392–410.
47. García-Acero M, Moreno-Niño O, Suárez-Obando F, Molina M, Manotas MC, Prieto JC, et al. Disorders of sex development: Genetic characterization of a patient cohort. Mol Med Rep. 2020;21:97.
48. Shukla V, Høffding MK, Hoffmann ER. Genome diversity and instability in human germ cells and preimplantation embryos. Semin Cell Dev Biol. 2021;113:132.
49. Batista R, Nishi M, Rodrigues A, Costa EM, Domenice S, Mendonca B. SUN-018 Epigenetic Loss of the PIWI/piRNA Machinery in Gonadal Tumors in Androgen Insensitivity Syndrome. J Endocr Soc 2019;3. https://doi.org/10.1210/JS.2019-SUN-018.
50. Marcel V, Hainaut P. p53 isoforms - a conspiracy to kidnap p53 tumor suppressor activity? Cell Mol Life Sci. 2009;66:391–406.
51. Craig AL, Blaydes JP, Burch LR, Thompson AM, Hupp TR. Dephosphorylation of p53 at Ser2O after cellular exposure to low levels of non-ionizing radiation. Oncogene. 1999;18:6305–6312.
52. Herbig U, Jobling WA, Chen BPC, Chen DJ, Sedivy JM. Telomere shortening triggers senescence of human cells through a pathway involving ATM, p53, and p21(CIP1), but not p16(INK4a). Mol Cell. 2004;14:501–513.
53. D'Adda Di Fagagna F, Reaper PM, Clay-Farrace L, Fiegler H, Carr P, Von Zglinicki T, et al. A DNA damage checkpoint response in telomere-initiated senescence. Nature. 2003;426:194–8.
54. Davoli T, de Lange T. Telomere-driven tetraploidization occurs in human cells undergoing crisis and promotes transformation of mouse cells. Cancer Cell. 2012;21:765–776.
55. Ohata M, Nakamura S, Fujita H, Isemura M. Prognostic implications of p21 (Waf1/Cip1) immunolocalization in multiple myeloma. Biomed Res. 2005;26. https://doi.org/10.2220/biomedres.26.91.
56. Winters ZE, Turley H, Harris AL, Norbury CJ, Hunt NC, Bradburn MJ et al. Subcellular localisation of cyclin B, Cdc2 and p21WAF1/CIP1 in breast cancer: Association with prognosis. Eur J Cancer 2001;37. https://doi.org/10.1016/S0959-8049(01)00327-6.
57. Nassour J, Schmidt TT, Karlseder J. Telomeres and Cancer: Resolving the Paradox. Annu Rev Cancer Biol 2021;5:59–77. https://doi.org/10.1146/annurev-cancerbio-050420-023410.
58. Choudhury S, Kolukula VK, Preet A, Albanese C, Avantaggiati ML. Dissecting the pathways that destabilize mutant p53: the proteasome or autophagy? Cell Cycle. 2013;12:1022–9.
59. Kruiswijk F, Labuschagne CF, Vousden KH. p53 in survival, death and metabolic health: a lifeguard with a licence to kill. Nat Rev Mol Cell Biol. 2015;16:393–405.
60. Burdette DL, Vance RE. STING and the innate immune response to nucleic acids in the cytosol. Nat Immunol 2012 14:1. 2012;14:19–26.
61. Trigunaite A, Dimo J, Jørgensen TN. Suppressive effects of androgens on the immune system. Cell Immunol 2015;294:87–94. https://doi.org/10.1016/j.cellimm.2015.02.004.
62. Brown NA, Miller G. Immunoglobulin expression by human B lymphocytes clonally transformed by Epstein Barr virus. J Immunol. 1982;128:24–9.
63. Wessel D, Flügge UI. A method for the quantitative recovery of protein in dilute solution in the presence of detergents and lipids. Anal Biochem. 1984;138:141–3.
64. Rappsilber J, Mann M, Ishihama Y. Protocol for micro-purification, enrichment, pre-fractionation and storage of peptides for proteomics using StageTips. Nat Protoc 2007 2:8. 2007;2:1896–1906.
65. Ditton HJ, Zimmer J, Kamp C, Rajpert-De Meyts E, Vogt PH. The AZFa gene DBY (DDX3Y) is widely transcribed but the protein is limited to the male germ cells by translation control. Hum Mol Genet. 2004;13:2333–2341.

ACKNOWLEDGEMENTS

We would like to thank Core Facility for Mass Spectrometry & Proteomics of University of Heidelberg for mass spectrometry analysis. Also, we would like to thank Prof. E. Alexandrova for the critical comments on the manuscript and TP53 work in particular.

AUTHOR CONTRIBUTIONS

MK initiated and supervised the project, performed experiments, analyzed data, supervised JZ and AS, and wrote the paper. JZ performed the experiments and analyzed the data. AS did telomere assay. PFH, JR, MH, MB, TS provided the patients material. ML performed mass spec analysis. TS obtained the funding. All authors commented on the paper.

FUNDING

Open Access funding enabled and organized by Projekt DEAL.

COMPETING INTERESTS

The authors declare no competing interests.

ADDITIONAL INFORMATION

Supplementary information The online version contains supplementary material available at https://doi.org/10.1038/s41420-023-01470-6.

Correspondence and requests for materials should be addressed to Maria Krivega.

Reprints and permission information is available at http://www.nature.com/reprints

Publisher's note Springer Nature remains neutral with regard to jurisdictional claims in published maps and institutional affiliations.